Nanoscale

PAPER

View Article Online
View Journal | View Issue

Cite this: *Nanoscale*, 2016, **8**, 12362

Injectable shear-thinning nanoengineered hydrogels for stem cell delivery

Ashish Thakur,[a] Manish K. Jaiswal,[a] Charles W. Peak,[a] James K. Carrow,[a] James Gentry,[a] Alireza Dolatshahi-Pirouz[b] and Akhilesh K. Gaharwar*[a,c,d]

Received 19th March 2016,
Accepted 23rd May 2016

DOI: 10.1039/c6nr02299e

www.rsc.org/nanoscale

Injectable hydrogels are investigated for cell encapsulation and delivery as they can shield cells from high shear forces. One of the approaches to obtain injectable hydrogels is to reinforce polymeric networks with high aspect ratio nanoparticles such as two-dimensional (2D) nanomaterials. 2D nanomaterials are an emerging class of ultrathin materials with a high degree of anisotropy and they strongly interact with polymers resulting in the formation of shear-thinning hydrogels. Here, we present 2D nanosilicate reinforced kappa–carrageenan (κCA) hydrogels for cellular delivery. κCA is a natural polysaccharide that resembles native glycosaminoglycans and can form brittle hydrogels *via* ionic crosslinking. The chemical modification of κCA with photocrosslinkable methacrylate groups renders the formation of a covalently crosslinked network (MκCA). Reinforcing the MκCA with 2D nanosilicates results in shear-thinning characteristics, and enhanced mechanical stiffness, elastomeric properties, and physiological stability. The shear-thinning characteristics of nanocomposite hydrogels are investigated for human mesenchymal stem cell (hMSC) delivery. The hMSCs showed high cell viability after injection and encapsulated cells showed a circular morphology. The proposed shear-thinning nanoengineered hydrogels can be used for cell delivery for cartilage tissue regeneration and 3D bioprinting.

Introduction

Tissue engineering aims to regenerate tissues and organs in three-dimensional (3D) space with precisely controlled microenvironments for tissue repair following a variety of disease pathologies.[1–3] Recently, there has been tremendous progress in developing injectable biomaterials for facile cellular encapsulation and delivery.[4–7] Shear-thinning injectable hydrogels are able to shield encapsulated cells from high shear forces, thereby improving the outcome of cell-based therapeutics.[8–10] Polymeric hydrogels are often used for cell delivery because they are a highly hydrated network and can mimic some of the characteristics of the native microenvironment.[11–14] However, the inability to retain structural integrity after injection limits their utility for various tissue-engineering applications. Hence designing injectable hydrogels with shear-thinning characteristics, high stiffness and an ability to maintain high cell viability after injection is imperative.[6,15,16]

A range of nanomaterials such as polymeric, carbon-based, metallic oxide and inorganic nanomaterials are incorporated within the polymeric network to obtain mechanically stiff and injectable hydrogels.[17–20] A new family of two-dimensional (2D) nanomaterials has been shown to have exceptional mechanical strength due to their ultrathin 2D structure.[21–24] These 2D nanomaterials have high structural anisotropy and surface-to-volume ratio and can interact with a range of polymers to result in stiff and tough hydrogels.[19–22] Although these 2D nanomaterials are in an early stage of development, they have shown potential in engineering multifunctional biomaterials for various medical applications including photothermal therapies, therapeutic delivery, tissue regeneration, bioimaging, and biosensors.[22]

Synthetic silicates, an ultrathin class of 2D nanomaterials, have been shown to strongly interact with synthetic and natural polymers due to their high surface-to-volume ratio, similar to other types of 2D nanomaterials.[25] These nanosilicates result in the formation of shear-thinning hydrogels when combined with long-chain polymers.[26–29] Our earlier work has shown high cyto- and bio-compatibility of these 2D nanosilicates (nSi).[26,30,31] Moreover, these 2D nanosilicates also interact with growth factors and are explored for tissue engineering[30] and therapeutic delivery.[32] Thus, by reinforcing polymeric hydrogels with these 2D nanosilicates, we can develop multifunctional hydrogels for biomedical and biotechnological applications.

[a]*Department of Biomedical Engineering, Texas A&M University, College Station, TX-77843, USA. E-mail: gaharwar@tamu.edu*
[b]*Technical University of Denmark, DTU Nanotech, Center for Nanomedicine and Theranostics, Kongens Lyngby, Region Hovedstaden, Denmark*
[c]*Department of Materials Sciences, Texas A&M University, College Station, TX-77843, USA*
[d]*Center for Remote Health Technologies and Systems, Texas A&M University, College Station, TX 77843, USA*

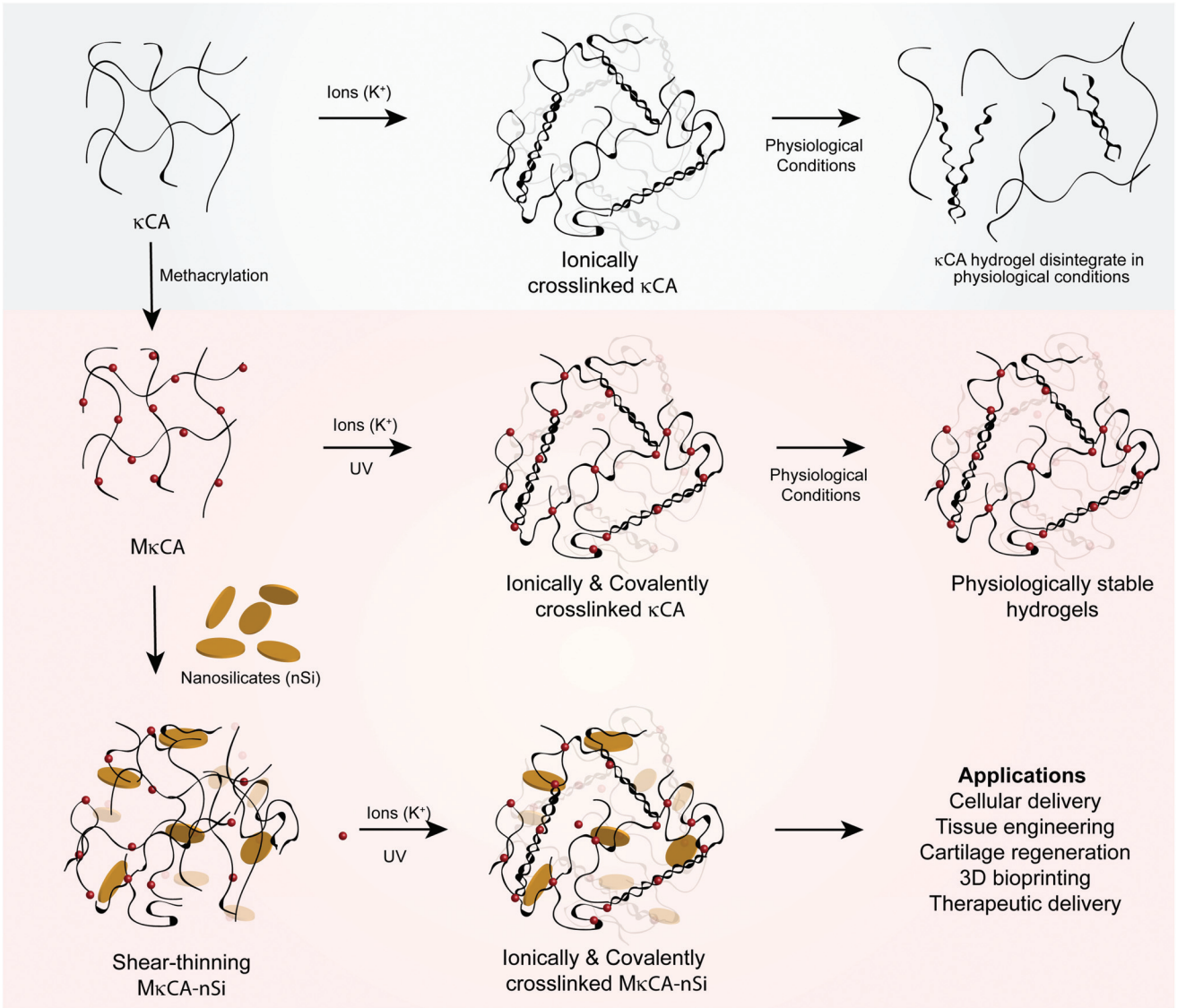

Fig. 1 Schematic outlining the design strategy to synthesize multifunctional nanocomposite hydrogels. κCA is predominantly crosslinked in the presence of potassium ions (sulphate groups interact with K^+ ions to drive a helical polymer conformation), which loses its mechanical stability under physiological conditions. Methacrylation of κCA results in a covalently crosslinkable polymer. The addition of nanosilicates provides shear thinning and bioactive properties to the polymer that can be used in various tissue engineering applications.

Here, we fabricate dual-crosslinked, mechanically robust kappa-carrageenan (κCA) hydrogels reinforced with 2D nanosilicates (Fig. 1). κCA is a natural polysaccharide that resembles native glycosaminoglycans (GAGs) such as chondroitin-4-sulphate and dermatan sulphate, which are major components of native extracellular matrices (ECM).[33–35] Previous studies have shown that in the presence of potassium ions (K^+), κCA can form brittle hydrogels.[36] Under physiological conditions, ionically crosslinked κCA loses its mechanical integrity, thereby limiting its biomedical application. To overcome these limitations, we propose to develop multifunctional dual-crosslinked κCA hydrogels. The chemical modification of the κCA backbone with a photocrosslinkable methacrylate group can provide enhanced structural stability under physiological conditions. Furthermore, by reinforcing the covalently crosslinked κCA network with 2D nanosilicates, an increase in the mechanical stiffness, elastomeric characteristics, and physiological stability is expected. The proposed multifunctional hydrogel networks have the potential to be used for delivery of cells, therapeutics for soft tissue regeneration, and 3D bioprinting.

Experimental

Synthesis of methacrylated kappa carrageenan (MκCA)

Kappa–carrageenan (κCA, Tokyo Chemical Industries, Japan), methacrylic anhydride (MA > 94%, Sigma Aldrich, USA), nanosilicates (nSi, Laponite XLG, BYK Additives Pvt. Ltd, USA), and

potassium chloride (KCl, Alfa-Aesar, USA) were used without further purification. For all experiments ultrapure water (resistivity > 18.2 MΩ cm) was used unless otherwise stated. Methacrylation of κCA was carried out by dissolving 2% κCA solution in 150 mL water and then vigorously mixing it with 12 mL of MA at 50 °C. To maintain the pH (>7.4), 5 M NaOH was added drop-wise. After 6 h the resulting precipitate was dialyzed using a cellulose dialysis membrane (Mol. Wt cut-off ~ 12–14 kDa) at 4 °C against ultrapure water for a week to remove any unreacted reagent and by-products (*e.g.* methacrylic acid). The dialyzed product was lyophilized and stored at −20 °C for further use.

Fabrication of dual crosslinked hydrogels

Prepolymer solutions of 2% κCA and MκCA were prepared in ultrapure water. Nanocomposites of MκCA with nanosilicates (MκCA–nSi) were fabricated by adding 1, 1.5 and 2 wt% of nSi. Samples were prepared by injecting the prepolymer solution in disc-shaped polydimethylsiloxane molds (7 mm diameter and 2 mm height). For κCA loaded solutions, 5% KCl was added to the molds until they were fully covered. Followed by 5 min incubation, the molds were gently agitated to remove hydrogels. Preparation of MκCA and MκCA–nSi dual crosslinked gels was achieved by 60 s of UV irradiation (1.69 mW cm^{-2}) prior to 5 min of KCl incubation.

Physiochemical and structural characteristics

To determine the physiological stability of the crosslinked network, the hydrogels were soaked in DPBS, and the wet weight was measured periodically up to 24 h. The stability and ion dependency of the κCA and its nanocomposites were assessed. The hydrogels were incubated in 5 mL 1× DPBS and incubated at 37 °C under static conditions. The wet weight of the hydrogels was measured at pre-determined time points (n = 5). Attenuated total infra-red reflection (ATR) was performed for nanocomposite hydrogels along with κCA using an ATR spectrophotometer (Bruker Vector 22, PIKE Technologies, USA). Prepolymer solutions were diluted to 10 ng mL^{-1} in ultrapure water for analysis of the zeta potential and hydrodynamic diameter (d_H) using a Zetasizer (Malvern ZEN3600, Malvern Instruments, USA). Methacrylation of κCA was confirmed by X-ray photoelectron spectroscopy (XPS, Omicron DAR 400) equipped with Mg (K_α) X-ray sources. Casa XPS software was then used for deconvolution of the peaks and for further analysis. The microporous structure of freeze-dried hydrogels was investigated using scanning electron microscopy (SEM, FEI Quanta 600) at 20 keV. The samples were coated with Pt/Pd for electron conductance. The pore sizes were further computed using ImageJ software (National Institute of Health).

Rheological and mechanical analysis

Rheological properties were characterized using a Physica MCR 301 rheometer (Anton Paar, USA). Gelation kinetics of prepolymer solutions of MκCA and MκCA–nSi under UV irradiation was investigated using a 10 mm parallel plate geometry at a gap of 0.3 mm. Fabricated gels were incubated in PBS (1×) for an hour and investigated under unconfined uniaxial compression using an ADMET eXpert 7600 single column testing system equipped with a 50 lb transducer. The samples were compressed with a strain rate of 1 mm min^{-1} up to 80% strain. The compressive modulus and energy dissipated per unit volume (toughness) were calculated for each composition (n = 5).

In vitro cellular behaviour & proliferation studies

Human mesenchymal stem cells (hMSCs) obtained from Lonza Inc. were cultured in growth media supplemented with 16.5% FBS and 1% streptomycin/penicillin (αMEM, Life Technologies, USA) at 37 °C under a 5% CO_2 atmosphere. hMSCs were encapsulated in prepolymer solutions containing κCA (2 wt/v%), MκCA (2 wt/v%), or MκCA–nSi (2 wt/v% MκCA and 2 wt/v% nanosilicates) at a density of 10^5 cells per gel. Cellular viability was assessed using Calcein AM for live cells and the ethidium homodimer for dead cells according to manufacturer's protocol (Life Technologies, USA). In a typical procedure, prepolymer solutions were physically mixed with the cells, injected using a flow rate of 1000 μL mL^{-1} with a 27-gauge needle, and covalently crosslinked to form hydrogels in a 48-well plate. All the samples were analysed in triplicate. After 24 and 72 h, the samples were washed with 1× DPBS, and incubated in stains for 30 min under physiological conditions. The stained samples were subsequently washed with 1× DPBS and imaged with a fluorescence microscope (Nikon, TE2000-S). Percent viability was calculated by using Image J (NIH) software. To determine the cell morphology, the encapsulated cells were stained by actin cytoskeletal staining (Phalloidin-Alexa 488, Invitrogen), which was performed according to the manufacturer's protocol and the nuclei were counterstained with propidium iodide (PI).

To evaluate the metabolic activity of seeded hMSCs on the nanocomposite hydrogel surface, the alamarBlue assay at 24 h and 72 h after seeding was performed. Furthermore, cellular activity was also analyzed through cell cycle analysis of the seeded hMSCs. Prior to seeding, the cells were synchronized under low serum conditions (αMEM with 1% FBS) for 24 h to bring them in the interphase. A similar number of cells were seeded on scaffolds under physiological culture conditions in triplicate. Following the time points – days 1 and 3 – the cells were trypsinized, collected and washed with 1× DPBS three times and eventually fixed in ice-cold ethanol for 30 minutes and maintained at 4 °C. The cells were then centrifuged and excess ethanol was decanted. Thereafter the cells were washed twice in 1× DPBS, re-suspended in 200 μL propidium iodide solution (40 μg mL^{-1}, 100 μg mL^{-1} RNase A and 0.01% Triton X-100), and incubated at 37 °C for 30 minutes. BD Accuri C6 flow cytometry was used for analysis of different cellular phase's population.

Statistical analysis

The data are presented as their means ± standard deviations of the experiments (n = 3, unless otherwise stated). Statistical

analysis was performed using the nonparametric test, one-way analysis of variance (ANOVA) with Tukey's *post-hoc* pairwise mean comparisons. The statistical significance was defined as $*p < 0.05$, $**p < 0.01$, $***p < 0.005$.

Results and discussion

Carrageenan (CA) is an anionic natural hydrophilic biopolymer extracted from seaweed and is available in many forms based on the chemical configuration.[37] It is widely used in several applications such as in gelling agents, wound healing, cell therapy, emulsifiers, and food enhancers.[38] Chemically each unit of CA is comprised of alternating disaccharide repeating subunits of 3-linked β-D-galactopyranose (G subunits) and 4-linked α-D-galactopyranose (D subunits). Based on the configuration and the number of sulfate groups in CA, it is divided into three major classes.[39,40] CA with one sulfate group forms kappa carrageenan (κCA), while with two and three it forms iota (γCA) and lambda carrageenan (λCA), respectively. Because of the structural resemblance with natural glycosaminoglycans (GAGs), κCA is the most widely used carrageenan polymer.[41] The network formation in κCA occurs by binding of cationic agents (*e.g.* K^+) to the sulfates present in the structural backbone.[40]

Chemical modification of kappa carrageenan (κCA)

To obtain a covalently crosslinked polymer network, we modified the κCA backbone with methacrylic anhydride (MA) to obtain methacrylated κCA (MκCA). The methacrylation of κCA was achieved on the primary and secondary hydroxyl groups of the two subunits of the polysaccharides (Fig. 2a). The chemical modification of κCA was confirmed using X-ray photoelectron spectra (XPS) analysis. Specifically, we obtained spectra for core-level carbon electron (C 1s) and oxygen electron (O 1s) for κCA, MκCA, and crosslinked MκCA (UV crosslinked). The atomic ratios of oxygen to carbon (O/C) and sulphur to oxygen (S/O) along with their individual values for κCA and MκCA were estimated from the area under the curve (Fig. 2b). In κCA the overall contribution from carbon is approx. three times that of oxygen (O/C, 0.32) and the overall contribution of oxygen is ten times that of sulphur (S/O, 0.10). Due to methacrylation, the methacrylic groups contributed to the oxygen content and the ratio of carbon is reduced to only two times that of oxygen (O/C, 0.52). Also S contribution is slightly enhanced (S/O, 0.16). After UV exposure, due to the formation

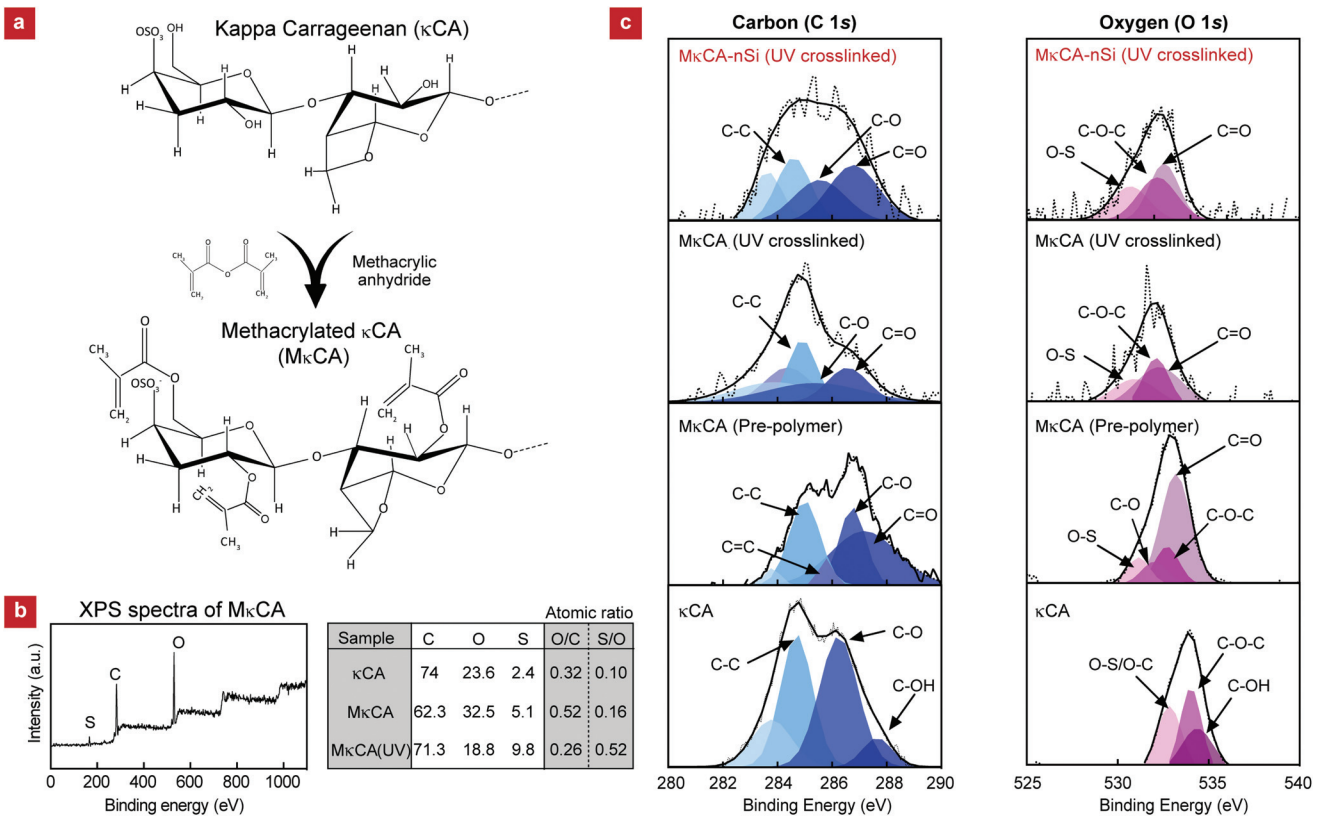

Fig. 2 Synthesis of photocrosslinkable MκCA. (a) The hydroxyl groups (–OH) in the polymer backbone were modified with photocrosslinkable methacrylates. (b) X-ray photoelectron spectroscopy (XPS) of MκCA and the atomic ratio (O/C and S/O) for κCA, MκCA and MκCA (UV crosslinked). (c) XPS confirms the modification of the –OH groups by methacrylates as indicated by the appearance of the C=O peak in MκCA. Upon UV exposure the C=C bond transforms into a covalent linkage C–C with neighbouring chains thus facilitating a cross-conjugated network formation. Addition of nSi does not alter the peak positions indicating their purely electrostatic interactions with the polymer network.

of the crosslinked gel *via* C–C, there occurs reduction in O owing to water formation as the by product (O/C, 0.26) suggesting an increase in carbon contribution up to four times that of oxygen, and the sulfur content increased to about fifty percent of that of oxygen (O/S, 0.52). The overall atomic ratio clearly corroborated the formation of the covalently crosslinked gel after UV exposure.

The deconvoluted peaks of the C 1s core-level for κCA show the presence of C–OH (287.8 eV), C–O (286.1 eV), and C–C at 284.7 eV (Fig. 2c). After methacrylation, additional peaks at 287.1 and 285.8 eV from MκCA (prepolymer) revealed the presence of C═O and C═C, which are attributed to methacryloyl. This confirms the successful methacrylation of the κCA backbone. MκCA was used to obtain the covalently crosslinked network after UV exposure in the presence of a photoinitiator (Irgacure 2959). After UV exposure, the C═C bonds from vinyl groups in MκCA disappear, indicating the formation of a covalently crosslinked network. The remaining peaks seen in the modified formulation exist from incomplete crosslinking; suggesting that some C═C might still be available. Similarly, XPS analysis of the core-level oxygen electron (O 1s) supports the covalent modification of κCA. For κCA, the presence of C–OH (534.5 eV) and C–O–C (534.2 eV) was observed. After methacrylation, the disappearance of the O 1s peak corresponding to C–OH and the appearance of a new peak (533.8 eV) attributed to C═O were observed. The O 1s peaks corresponding to O–C, O–S and C–O–C have shifted toward lower binding energies due to methacrylation. After UV exposure, the O 1s peaks remained nearly unchanged, as oxygen does not take part in subunit crosslinking and polymerization. The incorporation of nanosilicates (nSi) to MκCA showed a minimum effect on the crosslinking process. With the addition of 2% nSi the overall contour of the C 1s profile became broader, without affecting the peak position, confirming the electrostatic interaction between the nSi and MκCA backbone. Overall, XPS data confirm the chemical modification of κCA and formation of the covalently crosslinked network from MκCA upon UV exposure.

Nanosilicates strongly interact with MκCA

κCA is used as a thickening agent in various applications due to its ability to form a 3D double helix network that results in strong interactions between the sulphate groups present on the polymer backbone.[33] The chemical modification of the κCA backbone is expected to influence the sol–gel behaviour of the prepolymer network. Specifically, the addition of methacrylate side groups is expected to change the stacking of κCA polymer chains and disrupt the sol–gel behaviour. A solution of 2% κCA showed a "gel-like" behaviour at room temperature, while MκCA showed a "sol-like" behaviour (Fig. 3a). The addition of nanosilicates to MκCA results in "gel-like" characteristics of prepolymer solution.

We investigated the interaction between the polymer and nanosilicates *via* dynamic light scattering (DLS). The hydrodynamic diameter (d_H) of hydrated nanosilicates, κCA and MκCA was determined (Fig. 3b). The d_H for nanosilicates and MκCA was observed to be ~50 nm and ~380 nm, respectively. When they were combined together, the size of MκCA–nSi was ~100 nm (Fig. 3b). This can be attributed to the strong interaction of MκCA with the positively charged edge of nSi.

We further investigated these physical interactions *via* electrophoretic measurements. The zeta potentials for κCA, MκCA and nSi were −12.7 ± 2.1, −19.2 ± 1.8 and −28.1 ± 1.8 mV, respectively (Fig. 3b). The change in zeta potential between κCA and MκCA is attributed to the chemical modification of –OH on the κCA backbone with methacrylate groups, which renders the formation of $RCOO^-$ in aqueous media. Further, upon the addition of nanosilicates to MκCA, the zeta potential of MκCA–nSi increased to −34.8 ± 1.9 mV due to its strong interaction with nSi. Earlier studies have shown that nanosilicates are multi-charged particles (have a positively charged edge and a negatively charged surface).[31] Due to this it is expected that the negatively charged groups from MκCA will interact with the positively charged nSi surface (edge).

Both DLS and zeta studies, strongly support that nSi and MκCA strongly interact with each other. We should also note that both DLS and zeta measurements were performed using highly diluted solutions. When the concentration of MκCA and nSi are increased, it is expected that they will also alter rheological characteristics.

Nanosilicates provide shear-thinning characteristics and enhance physiological stability

To investigate the effect of electrostatic interactions on shear-thinning characteristics, we monitored the viscosity of κCA, MκCA and MκCA–nSi at different shear rates (0.01–100 s^{-1}). The viscosity decreased with the increasing shear rate for all prepolymer compositions (Fig. 3c). However due to the modification of κCA, a shear-thinning polymer, with methacrylate groups, the viscosity of MκCA was reduced. However, addition of nanosilicates, returned the shear-thinning behaviour of MκCA–nSi as revealed *via* the shear rheology of prepolymer solutions. This characteristic of MκCA–nSi renders its application for cell encapsulation and delivery, which requires shielding of the encapsulated cells from shear mechanical forces. Overall, this study indicates the shear-thinning ability of prepolymer solutions, particularly that of the nanocomposite.

Methacrylate functional groups permit covalent crosslinking, which occurs through UV-initiated free radical polymerization. The kinetics of crosslinking of MκCA in the presence and absence of nSi was determined using UV rheology. Upon UV exposure, MκCA readily polymerizes and forms a covalently crosslinked gel within 30 seconds while reaching the plateau (G') at approx. 1 kPa (Fig. 3d). The addition of nSi prolongs the crosslinking kinetics and the fully crosslinked network has more than four-fold increase in storage modulus (G'). The significant change in the G' of the crosslinked network indicates that the enhanced electrostatic interactions of nSi with the polymer chains contribute to the physical

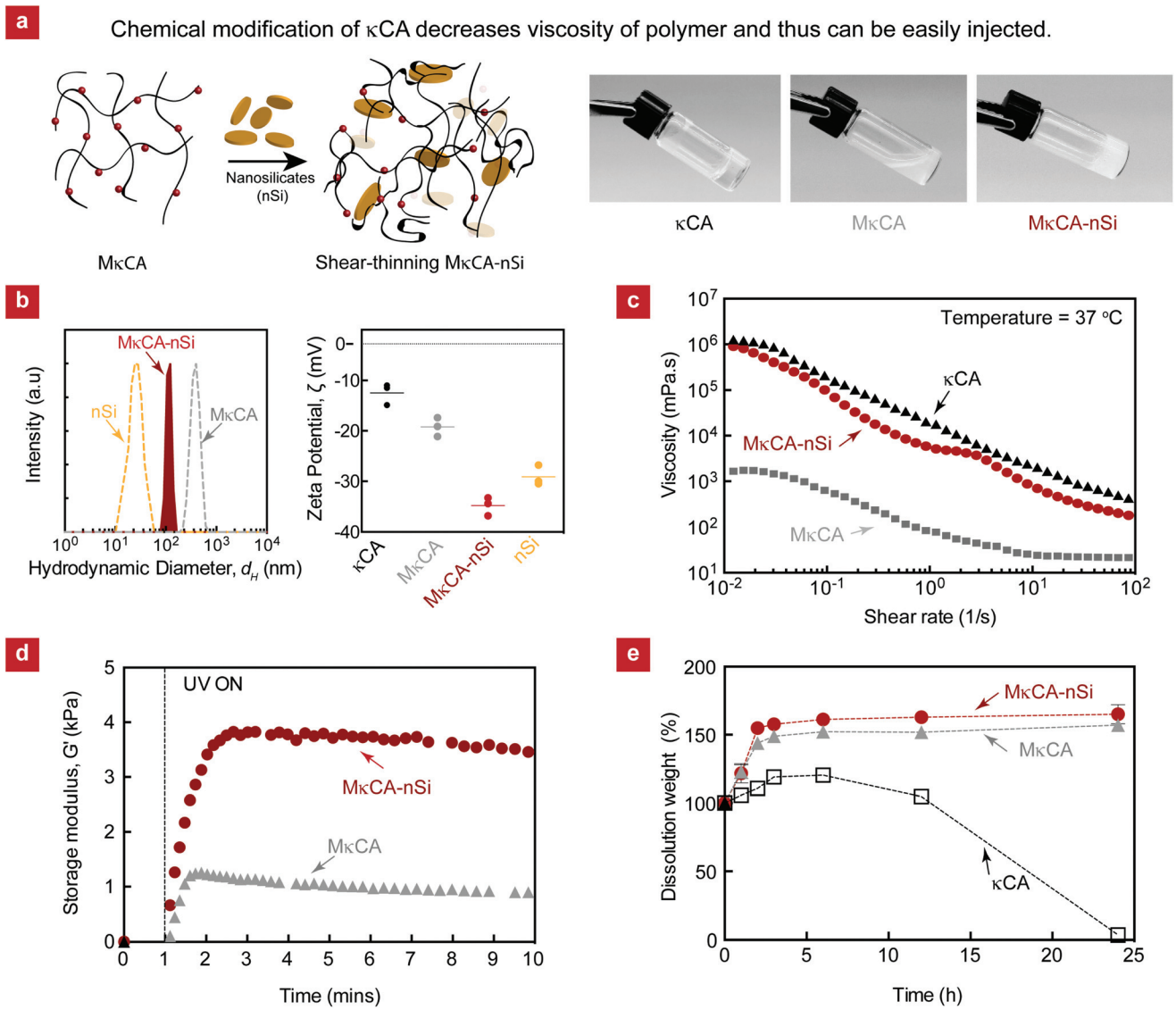

Fig. 3 Synthesis and fabrication of nanocomposite hydrogels. (a) The addition of nanosilicates (nSi) decreases the viscosity of prepolymer solution. (b) Hydrodynamic diameter (d_H) and zeta potential (ζ) measurements suggest strong interactions between nanosilciates (nSi) and κCA. (c) Both κCA and MκCA–nSi show shear thinning characteristics. (d) A significant increase in storage modulus (G') was also observed due to the addition of nSi to MκCA. (e) The enzymatic degradation kinetics confirmed enhanced network stability of hydrogels due to the addition of nanosilicates.

reinforcement of the covalently crosslinked polymer network. Moreover, facile crosslinking mechanisms also provide potential to quickly encapsulate and pattern cells using the microfabrication process.[11,42] Overall, the significant change in the shear modulus of κCA *via* methacrylation and further with nSi addition is vital for injectability.

The physiological stability of the hydrogel network plays an important role in determining its suitability for cell encapsulation and delivery applications. Pristine κCA hydrogels crosslinked with K^+ ions dissociate completely under physiological conditions within 24 h, due to ionic exchanges (Fig. 3e). The modification of κCA with methacrylate to obtain a crosslinked network enhanced the physiological stability of the network. No significant effect on stability was observed upon the addition of nSi to MκCA, indicating that nSi did not interfere with the network chemistry. It is also expected that the presence of nSi within the crosslinked network will prevent K^+ ions from diffusing out freely and hydrogels will be able to retain their mechanical stability.

Porous and interconnected nanocomposite network

To facilitate cell encapsulation, survival and further proliferation, the biomaterials should have interconnected porous networks to assist in nutrient and waste product transport. The ionically crosslinked κCA hydrogels form a porous micro-architecture. The change in pore sizes with methacrylation and further addition of nSi was analysed using Image J software for compositions (Fig. 4a). A significant change in the κCA pore

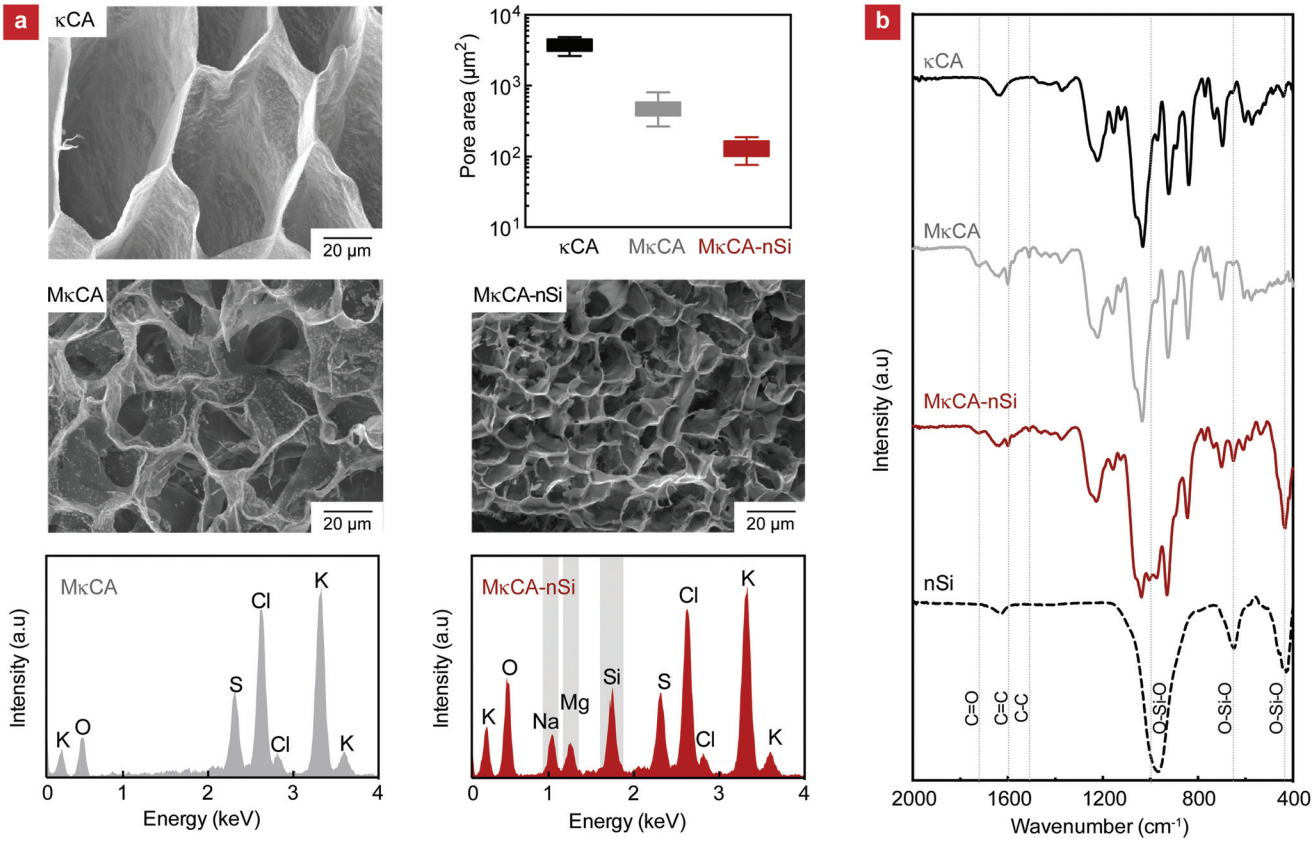

Fig. 4 Structural characterization of the nanocomposite network. (a) κCA shows a porous and interconnected network. The chemical modification of κCA results in a decrease in the pore size of the MκCA network. The addition of nSi further reduced the pore size due to enhanced interactions between the polymer and nanoparticles. The presence of nSi in the porous network was confirmed by EDS, as the peaks corresponding to Si, Mg, and Na were detected in the nanocomposites (MκCA–nSi). (b) The chemical modification of κCA was confirmed with FTIR spectra analysis which showed the bands corresponding to methacrylation (C═O), their crosslinking after UV exposure (C–C) and further presence of nSi in MκCA–nSi, respectively.

size was observed from about 3710 ± 745 μm^2 to 442 ± 145 μm^2 due to methacrylation (MκCA), which further reduced to 132 ± 35 μm^2 with the incorporation of 2% nSi (MκCA–nSi), suggesting an enhanced crosslinking *via* chemical and ionic interactions. The presence of minerals in nanocomposites was detected and confirmed using energy-dispersive X-ray spectroscopy (EDS). The typical EDS spectra indicated the presence of Na, Mg and Si as prime components of nanocomposites.

The presence of nanosilicates and the formation of a covalently crosslinked network were further verified by FTIR (Fig. 4b). The appearance of carbonyl >C═O at 1730 cm^{-1}, C═C at 1620 cm^{-1} and C–C at 1530 cm^{-1} confirmed the presence of the methacrylate group in MκCA, while the disappearance of the C═C peak in MκCA–nSi confirms the crosslinking of the prepolymer solution. The presence of the low intensity signal of C═C in crosslinked MκCA–nSi is due to incomplete crosslinking. The presence of nSi was confirmed by the appearance of O–S peaks which appear at 440 cm^{-1}, 660 cm^{-1} and 990 cm^{-1}. Overall, FTIR data confirm the XPS and EDS results.

Mechanically stiff, elastomeric and tough nanocomposite hydrogels

The mechanical properties of hydrogels govern the cellular response since the cells sense and respond to mechanical cues.[43] A range of soft and stiff hydrogels have shown to modulate the cell adhesion, proliferation and fate.[44,45] Ionically crosslinked κCA hydrogels are mechanically stiff initially, but quickly lose the mechanical integrity after being subjected to a hydrated microenvironment as a result of ion exchange. In addition, ionically crosslinked κCA hydrogels are not elastomeric (Fig. 5a) and this limits their use in biomedical applications. When subjected to cyclic stress, the ionically crosslinked κCA hydrogels do not recover to their original size and show significant plastic deformation. By incorporating methacrylate groups into the κCA backbone, a significant loss in mechanical stiffness was observed. This is similar to previous reports suggesting that the methacrylate groups present on the MκCA backbone limit the ability of the polymer to form ionic crosslinks.[46]

Covalently crosslinked MκCA hydrogels show elastomeric characteristics and sustain repeated mechanical deformation

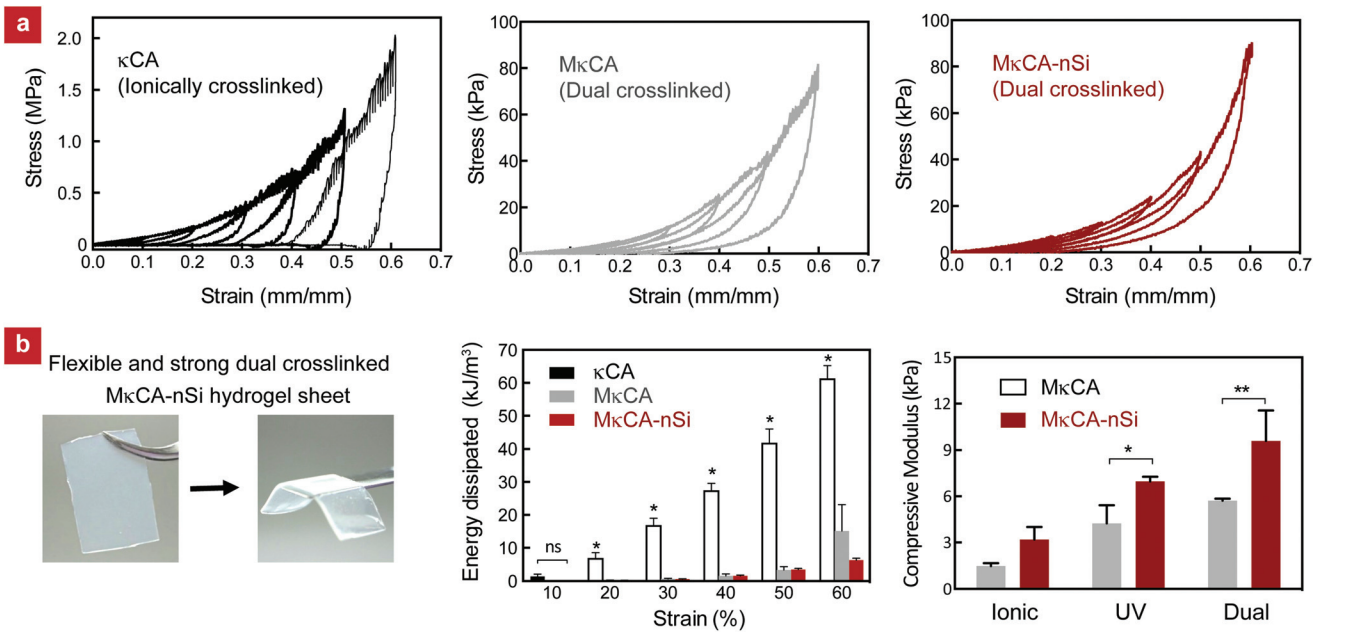

Fig. 5 Nanosilicates enhance the elasticity of the nanocomposite network. (a) The cyclic stress/strain curves for κCA, MκCA and MκCA–nSi show the elastomeric characteristics of the hydrogel network. Both MκCA and MκCA–nSi hydrogels recovery after cyclic deformation. (b) Image showing nanocomposite gels. The effect of addition of nanosilicates and the crosslinking mechanism on the compressive modulus of nanocomposite hydrogels.

with minimum plastic deformation. The addition of nSi to MκCA results in a mechanically stiff and flexible network. The addition of nSi improves the mechanical stiffness as well as elastic characteristics of gels at higher strains (Fig. 5a). The elasticity of the hydrogel network can be measured from the energy absorbed during the plastic deformation. The addition of nanosilicates to MκCA significantly reduces the energy absorbed by the nanocomposite network (6.3 ± 0.5 kJ m^{-3}), compared to MκCA (15.1 ± 7.7 kJ m^{-3}) at 60% strain. These characteristics of the nanocomposite hydrogels highlight their elastomeric properties, which play a pivotal role in tissue engineering applications, as this enables materials with enough resistance to bear the dynamic stress without being deformed at the site of interest.

The effect of different crosslinking mechanisms, such as ionic (physical crosslinking), UV (chemical crosslinking) and dual (both ionic and covalent), was investigated for MκCA and MκCA–nSi (Fig. 5b). The results suggest that the chemical crosslinking (mediated by UV) is more effective than the physical crosslinking method (mediated by K^+ ions) in order to fabricate stiffer MκCA hydrogels. Specifically, UV crosslinked hydrogels have a significantly higher compressive modulus (4.2 ± 1.2 kPa) compared to the ionically crosslinked hydrogels (1.5 ± 0.2 kPa) for MκCA hydrogels. The addition of nSi to MκCA hydrogels showed a similar increase in modulus from 3.2 ± 0.8 kPa (ionically) to 7.0 ± 0.3 kPa for UV crosslinked hydrogels. The dual crosslinking (UV and ionic) results in a further increase in the compressive modulus for MκCA (5.7 ± 0.1 kPa) and MκCA–nSi (9.6 ± 2.0 kPa) when compared to either covalent or ionically crosslinked hydrogels. Thus, the addition of nSi to MκCA results in an increase in the compressive moduli and the dual crosslinking mechanism is effective compared to either covalent or ionically crosslinked hydrogels.

Nanocomposites support cellular encapsulation and proliferation

Shear-thinning and injectable hydrogels can be used for minimally invasive therapies and 3D printing.[6,47–49] Injectable hydrogels have been shown to protect encapsulated cells from the damaging effects of the extensional flow.[6,7,49] We expect that the shear-thinning characteristics of nanocomposite hydrogels can be explored for these applications in the future. Due to faster dissolution of κCA under physiological conditions, we performed cell studies only with dual crosslinked hydrogels. We have investigated the effect of shear forces on the cells by encapsulating hMSCs within prepolymer solutions (MκCA, and MκCA–nSi) and injecting through a 27-gauge syringe (Fig. 6a). The encapsulated hMSCs showed high viability after injection (>80%), when stained with calcein AM (live cells) and the ethidium homodimer (dead cells) (Fig. 6b).

The effect of nanosilicates on cell spreading was monitored over a period of 7 days. hMSCs encapsulated within hydrogel networks showed a circular morphology (Fig. 6c), indicating that these compositions can be used for hMSC delivery for cartilage regeneration. Our results are consistent with earlier studies, which have shown that κCA-based hydrogels do not support cell spreading.

No significant effect of nanosilicate addition to κCA was observed on metabolic activities of the seeded cells (Fig. 6d).

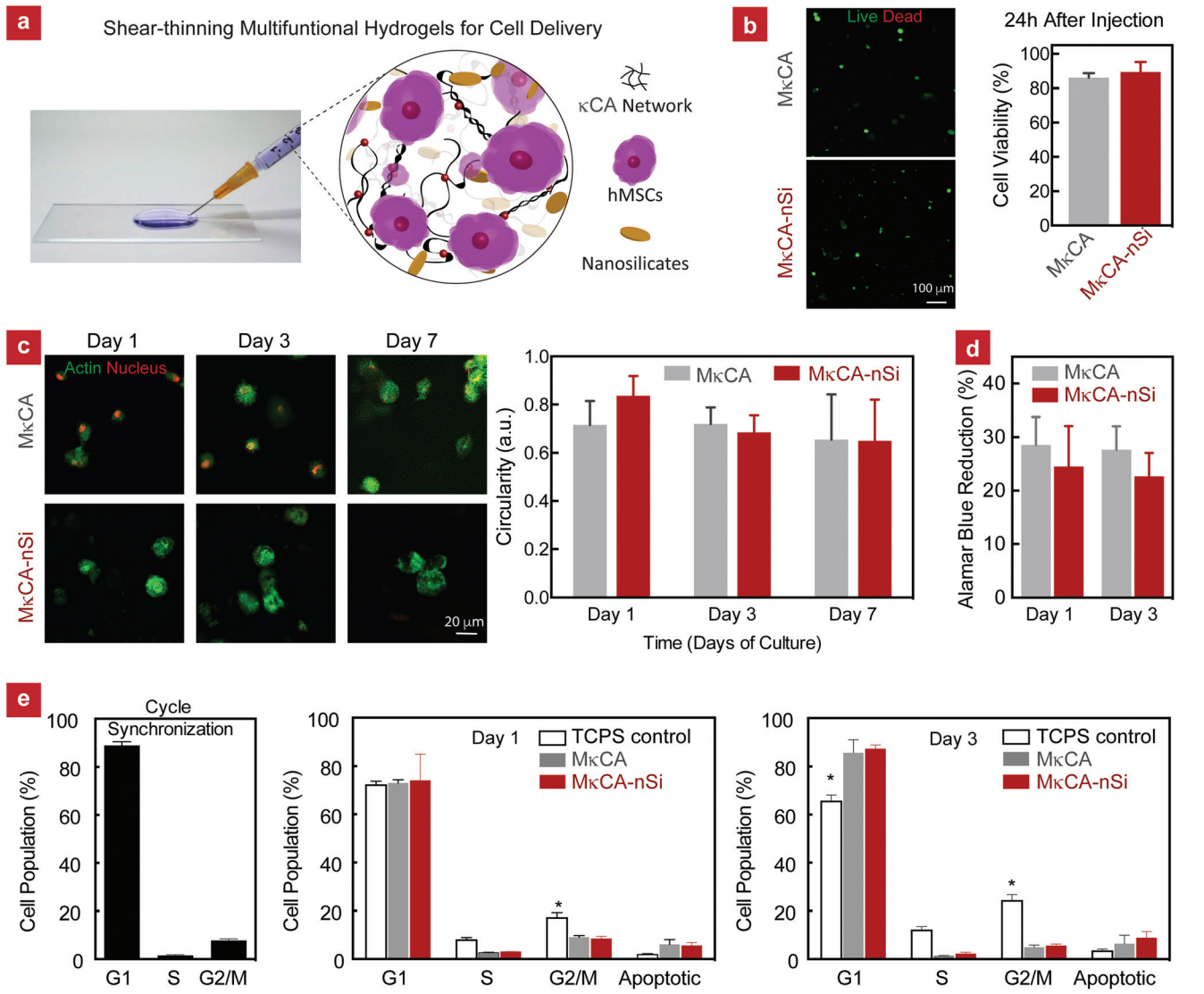

Fig. 6 *In vitro* evaluation of the nanocomposite network for cell delivery. (a) Nanocomposite hydrogels can be used to encapsulate and deliver cells due to their shear-thinning characteristics. (b) MκCA and MκCA–nSi show high viability (>80%) of encapsulated hMSCs after injection using a 27-gauge syringe. (c) Effect of nanosilicates on cell morphology was monitored by actin cytoskeleton staining over a period of 7 days. No significant effect was observed on cell circularity due to nanosilciates. (d) AlamarBlue assay showed no significant change in the metabolic activity of encapsulated cells in MκCA and MκCA–nSi. (e) Cell cycle analysis with about 90% cell synchronized exhibited minimal promotion in proliferation as more than 80% remained in the G0/G1 phase in MκCA and MκCA–nSi gels following 24 h (Day 1) and 72 h (Day 3) of encapsulation.

This might be attributed to the limited presence of cell adhesion sites within the nanocomposite hydrogels. A further investigation on the cell behaviour based on the cell cycle revealed that both MκCA and MκCA–nSi did not cause any adverse effect and no apoptotic cells were observed even after day 3 (Fig. 6e). The results also suggested that most of the cells were in the G1/G0 phase. For cartilage tissue engineering, limited cell adhesion and circular morphology are preferred and thus the proposed nanocomposites are expected to have application in cell delivery for cartilage tissue regeneration. In future, we will explore the ability of these nanocomposites to guide chondrogenic differentiation of encapsulated stem cells.

Although the addition of nanoparticles increases the mechanical stiffness of nanocomposite hydrogels, no significant change in cell morphology, spreading and metabolic activities was observed. This is in contrast to earlier reported studies, where an increase in mechanical stiffness of gelatin-based hydrogels supported cell spreading.[45,50–52] The contradiction with other studies is due to the use of κCA, which is shown to be non-cell adhesive, as the polysaccharide lacks any inherent cell-binding moieties. This morphological control may stimulate hMSC differentiation towards chondrogenic lineages.[44] In addition, previous reports have demonstrated that κCA-based hydrogels promote chondrogenic differentiation of stem

cells.[53,54] Overall, shear-thinning MκCA–nSi can be used for cell delivery for cartilage regeneration.

Conclusions

We developed dual-crosslinked, mechanically robust κCA hydrogels reinforced with 2D nanosilicates. The modification of the κCA backbone with the methacrylate group results in a photocrosslinkable hydrogel network (MκCA) with improved physiological stability and mechanical integrity. The addition of nanosilicates to MκCA results in shear-thinning characteristics, indicating the ability of nanosilicates to interact strongly with MκCA polymer chains and rendering injectability to pre-polymer solution for cell delivery. The nanosilicates further reinforced the polymeric networks to enhance physiological stability and elastomeric characteristics. Moreover, encapsulation of cells within the shear-thinning nanocomposites demonstrated high cell viability after injection. The encapsulated cells have round shaped morphology for over a week, indicating that this nanoengineered system has the potential to be used for the delivery of cells for cartilage tissue regeneration as well as 3D bioprinting.

Acknowledgements

AKG would like to acknowledge funding support from the Texas Engineering Experiment Station and Texas A&M University Seed Grant. We would like to thank Ramanathan Yegappan for his help. AT, MKJ and AKG conceptualized the idea and designed the project. AT, MKJ, CWP, JKC and JG performed the experiments and analysed the results. All the authors contributed in writing and revising the manuscript.

Notes and references

1 R. Langer and J. P. Vacanti, *Science*, 1993, **260**, 920–926.
2 M. Lutolf and J. Hubbell, *Nat. Biotechnol.*, 2005, **23**, 47–55.
3 E. A. Makris, A. H. Gomoll, K. N. Malizos, J. C. Hu and K. A. Athanasiou, *Nat. Rev. Rheumatol.*, 2015, **11**, 21–34.
4 A. M. Rosales and K. S. Anseth, *Nat. Rev. Mater.*, 2016, **1**, 15012.
5 J.-A. Yang, J. Yeom, B. W. Hwang, A. S. Hoffman and S. K. Hahn, *Prog. Polym. Sci.*, 2014, **39**, 1973–1986.
6 L. Yu and J. Ding, *Chem. Soc. Rev.*, 2008, **37**, 1473–1481.
7 J. A. Burdick, R. L. Mauck and S. Gerecht, *Cell Stem Cell*, 2016, **18**, 13–15.
8 M. Nikkhah, F. Edalat, S. Manoucheri and A. Khademhosseini, *Biomaterials*, 2012, **33**, 5230–5246.
9 P. Zorlutuna, N. Annabi, G. Camci-Unal, M. Nikkhah, J. M. Cha, J. W. Nichol, A. Manbachi, H. Bae, S. Chen and A. Khademhosseini, *Adv. Mater.*, 2012, **24**, 1782–1804.
10 B. A. Aguado, W. Mulyasasmita, J. Su, K. J. Lampe and S. C. Heilshorn, *Tissue Eng., Part A*, 2012, **18**, 806–815.
11 A. Khademhosseini and R. Langer, *Biomaterials*, 2007, **28**, 5087–5092.
12 A. M. Kloxin, C. J. Kloxin, C. N. Bowman and K. S. Anseth, *Adv. Mater.*, 2010, **22**, 3484–3494.
13 B. V. Slaughter, S. S. Khurshid, O. Z. Fisher, A. Khademhosseini and N. A. Peppas, *Adv. Mater.*, 2009, **21**, 3307–3329.
14 S. Sant, M. J. Hancock, J. P. Donnelly, D. Iyer and A. Khademhosseini, *Can. J. Chem. Eng.*, 2010, **88**, 899–911.
15 J. A. Burdick and W. L. Murphy, *Nat. Commun.*, 2012, **3**, 1269.
16 D. L. Alge and K. S. Anseth, *Nat. Mater.*, 2013, **12**, 950–952.
17 J. K. Carrow and A. K. Gaharwar, *Macromol. Chem. Phys.*, 2015, **216**, 248–264.
18 P. Kerativitayanan, J. K. Carrow and A. K. Gaharwar, *Adv. Healthcare Mater.*, 2015, **4**, 1600–1627.
19 A. K. Gaharwar, N. A. Peppas and A. Khademhosseini, *Biotechnol. Bioeng.*, 2014, **111**, 441–453.
20 A. Paul, *Nanomedicine*, 2015, **10**, 1371–1374.
21 S. Goenka, V. Sant and S. Sant, *J. Controlled Release*, 2014, **173**, 75–88.
22 D. Chimene, D. L. Alge and A. K. Gaharwar, *Adv. Mater.*, 2015, **27**, 7261–7284.
23 A. Paul, A. Hasan, H. A. Kindi, A. K. Gaharwar, V. T. Rao, M. Nikkhah, S. R. Shin, D. Krafft, M. R. Dokmeci and D. Shum-Tim, *ACS Nano*, 2014, **8**, 8050–8062.
24 S. Kumar, S. Raj, K. Sarkar and K. Chatterjee, *Nanoscale*, 2016, **8**, 6820–6836.
25 J. I. Dawson and R. O. Oreffo, *Adv. Mater.*, 2013, **25**, 4069–4086.
26 A. K. Gaharwar, R. K. Avery, A. Assmann, A. Paul, G. H. McKinley, A. Khademhosseini and B. D. Olsen, *ACS Nano*, 2014, **8**, 9833–9842.
27 J. R. Xavier, T. Thakur, P. Desai, M. K. Jaiswal, N. Sears, E. Cosgriff-Hernandez, R. Kaunas and A. K. Gaharwar, *ACS Nano*, 2015, **9**, 3109–3118.
28 C. Peak, J. Carrow, A. Thakur, A. Singh and A. Gaharwar, *Cell. Mol. Bioeng.*, 2015, **8**, 404–415.
29 W. E. Hennink and C. F. van Nostrum, *Adv. Drug Delivery Rev.*, 2002, **54**, 13–36.
30 A. K. Gaharwar, S. M. Mihaila, A. Swami, A. Patel, S. Sant, R. L. Reis, A. P. Marques, M. E. Gomes and A. Khademhosseini, *Adv. Mater.*, 2013, **25**, 3329–3336.
31 B. Ruzicka, E. Zaccarelli, L. Zulian, R. Angelini, M. Sztucki, A. Moussaïd, T. Narayanan and F. Sciortino, *Nat. Mater.*, 2011, **10**, 56–60.
32 R. Waters, S. Pacelli, R. Maloney, I. Medhi, R. P. H. Ahmed and A. Paul, *Nanoscale*, 2016, **8**, 7371–7376.
33 V. L. Campo, D. F. Kawano, D. B. da Silva and I. Carvalho, *Carbohydr. Polym.*, 2009, **77**, 167–180.
34 L. Li, R. Ni, Y. Shao and S. Mao, *Carbohydr. Polym.*, 2014, **103**, 1–11.
35 J. Venkatesan, B. Lowe, S. Anil, P. Manivasagan, A. A. A. Kheraif, K.-H. Kang and S.-K. Kim, *Starch - Stärke*, 2015, **67**, 381–390.

36 A.-M. Hermansson, E. Eriksson and E. Jordansson, *Carbohydr. Polym.*, 1991, **16**, 297–320.
37 M. R. Mangione, D. Giacomazza, D. Bulone, V. Martorana, G. Cavallaro and P. L. San Biagio, *Biophys. Chem.*, 2005, **113**, 129–135.
38 A. Trius and J. G. Sebranek, *Crit. Rev. Food Sci. Nutr.*, 1996, **36**, 69–85.
39 S. H. Moon and S. J. Parulekar, *Biotechnol. Prog.*, 1991, **7**, 516–525.
40 L. Piculell, J. Borgstrom, I. S. Chronakis, P. O. Quist and C. Viebke, *Int. J. Biol. Macromol.*, 1997, **21**, 141–153.
41 S. M. Mihaila, E. G. Popa, R. L. Reis, A. P. Marques and M. E. Gomes, *Biomacromolecules*, 2014, **15**, 2849–2860.
42 P. Zorlutuna, N. Annabi, G. Camci-Unal, M. Nikkhah, J. M. Cha, J. W. Nichol, A. Manbachi, H. Bae, S. Chen and A. Khademhosseini, *Adv. Mater.*, 2012, **24**, 1782–1804.
43 W. L. Murphy, T. C. McDevitt and A. J. Engler, *Nat. Mater.*, 2014, **13**, 547–557.
44 A. J. Engler, S. Sen, H. L. Sweeney and D. E. Discher, *Cell*, 2006, **126**, 677–689.
45 M. K. Jaiswal, J. R. Xavier, J. K. Carrow, P. Desai, D. Alge and A. K. Gaharwar, *ACS Nano*, 2016, **10**, 246–256.
46 S. M. Mihaila, A. K. Gaharwar, R. L. Reis, A. P. Marques, M. E. Gomes and A. Khademhosseini, *Adv. Healthcare Mater.*, 2013, **2**, 895–907.
47 C. B. Highley, C. B. Rodell and J. A. Burdick, *Adv. Mater.*, 2015, **27**, 5075–5079.
48 D. Chimene, L. K. Kimberly, R. R. Kaunas and A. K. Gaharwar, *Ann. Biomed. Eng.*, 2016, **44**, 2090–2102.
49 L. Cai, R. E. Dewi and S. C. Heilshorn, *Adv. Funct. Mater.*, 2015, **25**, 1344–1351.
50 C. W. Peak, J. K. Carrow, A. Thakur, A. Singh and A. K. Gaharwar, *Cell. Mol. Bioeng.*, 2015, **8**, 404–415.
51 T. Thakur, J. R. Xavier, L. Cross, M. K. Jaiswal, E. Mondragon, R. Kaunas and A. K. Gaharwar, *J. Biomed. Mater. Res., Part A*, 2016, **104**, 879–888.
52 A. K. Gaharwar, P. J. Schexnailder, B. P. Kline and G. Schmidt, *Acta Biomater.*, 2011, **7**, 568–577.
53 E. Popa, R. Reis and M. Gomes, *Biotechnol. Appl. Biochem.*, 2012, **59**, 132–141.
54 E. G. Popa, S. G. Caridade, J. F. Mano, R. L. Reis and M. E. Gomes, *J. Tissue Eng. Regener. Med.*, 2015, **9**, 550–563.